Nearsurface seismic properties for elastic wavefield decomposition: Estimates based on multicomponent land and seabed recordings

GEOPHYSICS, VOL. 68, NO. 6 (NOVEMBER-DECEMBER 2003); P. 2073–2081, 8 FIGS.
10.1190/1.1635061

Near-surface seismic properties for elastic wavefield decomposition: Estimates based on multicomponent land and seabed recordings

Remco Muijs*, Johan O. A. Robertsson‡, Andrew Curtis**, and Klaus Holliger*

ABSTRACT

Accurate knowledge of the seismic material properties in the immediate vicinity of the receivers represents a prerequisite for elastic wavefield decomposition. We present strategies for estimating the elastic material properties for both land and seabed multicomponent seismic data. The proposed scheme for land data requires dense multicomponent geophone configurations, which allow spatial wavefield derivatives to be explicitly calculated. The required information can be obtained with four three-component surface geophones positioned at the corners of a square, and a fifth geophone buried at a shallow depth below the center of the square. The technique yields local estimates of the near-surface P- and S-wave velocities, but the density cannot be constrained. Using a similar approach for four-component (three orthogonal components of particle velocity plus pressure) seabed recordings allows the P- and S-wave velocities as well as the density of the seafloor to be estimated. In this case, the proposed scheme does not require buried geophones, and it is applicable to multicomponent data recorded in routine seabed surveys. Compared to existing techniques, the new method allows the elastic seafloor properties to be more accurately determined, and it does not rely critically on the inclusion of large-offset data. Numerical tests indicate that the proposed schemes are robust and yield accurate results, provided that the signal used for the inversion contains sufficient horizontal energy and can be clearly identified and separated from other signals. Although the schemes are designed for application on the first arrivals, they are, in principle, applicable to any data window containing isolated P- or S-arrivals. The proposed scheme is successfully applied to a seabed data set acquired in the North Sea. In contrast, the application on a multicomponent land data set was unsuccessful, because of strong receiver-to-receiver variations in amplitude and phase, probably caused by differences in coupling and instrument response.

INTRODUCTION

Decomposition of an elastic wavefield into its up- and downgoing P- and S-wave components allows crisper and more realistic images of the subsurface to be obtained and thus facilitates the interpretation of seismic data (e.g., Haugen et al., 1998; Caldwell, 1999). Existing decomposition schemes (e.g., Wapenaar et al., 1990; Amundsen et al., 2000; Robertsson and Curtis, 2002) require accurate information about the elastic properties in the immediate vicinity of the receivers as input. Commonly, this information is determined from the results of high-resolution refraction surveys. This conventional approach suffers from three important drawbacks: (1) it is usually unclear which part of the subsurface is resolved by the refracted P-waves, (2) the density of the near surface cannot be resolved and the S-wave velocity is at best only poorly constrained, and (3) the additional recordings increase the overall acquisition costs of the investigation.

Dispersion analysis of interface waves in land or marine data (e.g., Allnor et al., 1997; Roth and Holliger, 1999; Muyzert, 2000) is an alternative approach for estimating the elastic properties of the near surface. Unfortunately, the bandwidth of the signal used to constrain the seismic velocities is typically much lower than that of the signal of interest and the properties obtained using these techniques may not be those required for wavefield decomposition.

Robertsson and Muyzert (1999) presented an explicit P/S-splitting technique based on dense volumetric recordings of the

Manuscript received by the Editor September 2, 2002; revised manuscript received February 5, 2003.
*Institute of Geophysics, Swiss Federal Institute of Technology, ETH-Hönggerberg, CH-8093 Zurich, Switzerland. E-mail: remco@aug.ig.erdw.ethz.ch; holliger@aug.ig.erdw.ethz.ch.
‡Schlumberger Cambridge Research, High Cross, Madingley Road, Cambridge CB3 0EL, United Kingdom. E-mail: jrobertsson@cambridge.oilfield.slb.com.
**Schlumberger Cambridge Research, High Cross, Madingley Road, Cambridge CB3 0EL, United Kingdom and School of GeoSciences, Edinburgh University, Edinburgh EH9 3JG, United Kingdom. E-mail: curtis@cambridge.oilfield.slb.com.

wavefield. Their approach allows the total P- and S-wavefields to be separated without a priori information about the near surface. Up- and downgoing waves, however, cannot be distinguished using this technique. Complete decomposition of the wavefield into up- and downgoing P- and S-waves does require the elastic properties in the immediate vicinity of the receivers to be estimated. Curtis and Robertsson (2002) proposed an inversion scheme with which this information can be obtained from multicomponent land data recorded in dense receiver patterns. A major advantage of their method is the localized manner in which P- and S-wave velocities are estimated. Moreover, the elastic properties obtained using this technique are those that control the interaction of the up- and downgoing wavefields at the free surface. As such, they represent exactly those wave velocities required for wavefield decomposition. The method proposed by Curtis and Robertsson (2002) requires the explicit computation of higher order spatial derivatives, which renders the technique very susceptible to inaccuracies in the recorded amplitudes and noise.

In the first half of this paper, we present a technique for estimating near-surface P- and S-wave velocities on land without the need for higher order spatial derivatives. The method is based on angle-dependent estimates of the reflection and conversion coefficients using isolated events recorded by dense patterns of multicomponent geophones. The proposed scheme shares the advantages described above of the technique presented by Curtis and Robertsson (2002), but is computationally more efficient, requires the deployment of fewer geophones, and is inherently less susceptible to data inaccuracies and noise.

Commonly, the elastic properties of the sea floor are estimated from amplitude variation with offset (AVO) analyses of the sea-floor reflection coefficient, which can be computed from seabed recordings of pressure and the vertical component of particle velocity (e.g., Amundsen and Reitan, 1994, 1995; Schalkwijk et al., 1999). In a multicomponent ocean-bottom seismic experiment, three orthogonal components of particle velocity and pressure are routinely recorded; the above techniques, therefore, do not make full use of the measured data. In the second half of this paper, we propose a method for estimating the elastic properties of the sea floor that includes the information contained in all recorded data components simultaneously in the inversion procedure. This extension allows the sea-floor properties to be more accurately constrained and avoids the necessity for incorporating wide-angle data. In contrast to the formulation for land data, estimating the P- and S-wave velocities and density of the seabed does not require buried receivers and the method may be applied to multicomponent [four-component (4-C)] data recorded in routine seabed experiments.

We first outline the common theoretical framework for the proposed methods. The resulting algorithms for land and seabed recordings are then tested on synthetic data and finally applied to observed data sets.

ESTIMATING NEAR-SURFACE SEISMIC MATERIAL PROPERTIES FROM LAND SEISMIC RECORDINGS

In the following, we assume that the first arrival is separated in time from later arriving reflected and refracted waves, such that a time-offset window containing only this event can be chosen. At the free surface, the incident P-wave Φ_i will generate reflected P- and S-waves Φ_r and Ψ_r, respectively. The relation between the up- and downgoing wave components is well understood and is commonly expressed in terms of reflection and conversion coefficients R_{PP} and R_{PS}, respectively. These coefficients are functions of the horizontal slowness and the elastic properties of the medium in the immediate vicinity of the receivers (Aki and Richards, 2002):

$$R_{PP} = \frac{\Phi_r}{\Phi_i} = \frac{4\beta^4 p^2 q_p q_s - (1-2\beta^2 p^2)^2}{4\beta^4 p^2 q_p q_s + (1-2\beta^2 p^2)^2}, \quad (1)$$

$$R_{PS} = \frac{\Psi_r}{\Phi_i} = \frac{-4\beta^4 p q_p (1-2\beta^2 p^2)}{4\beta^4 p^2 q_p q_s + (1-2\beta^2 p^2)^2}, \quad (2)$$

where α and β are the P- and S-wave velocities, respectively, p is the horizontal slowness, and q_p and q_s are the vertical slownesses of the incident P-wave and the converted S-wave, respectively. The vertical slownesses can be expressed in terms of the horizontal slowness and seismic velocities:

$$q_p = (\alpha^{-2} - p^2)^{1/2}, \quad (3)$$

$$q_s = (\beta^{-2} - p^2)^{1/2}. \quad (4)$$

For a homogeneous isotropic medium, Helmholtz separation relates the above P- and S-wave components to the three components of particle velocity, v_x, v_y, and v_z, recorded by a multicomponent geophone:

$$\mathbf{v} = \nabla(\Phi_i + \Phi_r) + \nabla \times \Psi_r, \quad (5)$$

where $\mathbf{v} = (v_x, v_y, v_z)^T$. From the above sets of equations, it can be shown that the particle velocities recorded on the free surface due to an incident plane P-wave propagating with slowness p are related as (Aki and Richards, 2002):

$$v_h(\mathbf{x}_0) = \frac{p(R_{PP}+1) - q_s R_{PS}}{q_p(R_{PP}-1) + p R_{PS}} v_z(\mathbf{x}_0), \quad (6)$$

where $v_h(\mathbf{x}_0)$ denotes the radial component of particle velocity recorded at position $\mathbf{x}_0$ at the free surface.

Because seismic energy typically arrives at the free surface at small angles of incidence, equation (6) represents only a weak constraint on the near-surface seismic velocities. However, Robertsson and Curtis (2002) have shown that the free-surface boundary conditions imply

$$\partial_z v_z(\mathbf{x}_0) = \left(1 - \frac{2\beta^2}{\alpha^2}\right)[\partial_x v_x(\mathbf{x}_0) + \partial_y v_y(\mathbf{x}_0)], \quad (7)$$

where ∂_x, ∂_y, and ∂_z are partial derivatives in the x-, y-, and z-directions, respectively. Inversion schemes aimed at estimating the elastic properties of the near surface from equations (6) and (7) require local estimates of the horizontal and vertical derivatives of particle velocity centered at the free surface. Such information can be obtained using a dense configuration of at least four three-component (3-C) geophones, one of which is buried just below the surface. Possible acquisition geometries include the tetrahedral configuration proposed by Robertsson and Muyzert (1999) or the pyramid-shaped configuration shown in Figure 1a (Muijs et al., 2000). Subtracting the recordings of the buried and surface geophones will yield vertical spatial derivatives of particle velocity centered a small distance below the free surface. Curtis and Robertsson (2002)

have shown that nonuniform centering of spatial derivatives can introduce significant inaccuracies for spacings as small as 12.5 cm. One approach to correct for this effect is to use a Taylor expansion of the wavefield about $\mathbf{x}_0$:

$$\partial_z v_z(\mathbf{x}_0) = \left[\frac{v_z(\mathbf{x}_0+\boldsymbol{\Delta}) - v_z(\mathbf{x}_0)}{\Delta}\right] - \frac{\Delta}{2}\partial_{zz} v_z(\mathbf{x}_0) + O(\Delta^2), \tag{8}$$

where $\boldsymbol{\Delta}$ is the vector $[0, 0, \Delta]$ pointing downwards. Assuming that the receiver pattern is sufficiently small for the wave components to be regarded as plane waves, the second-order vertical derivative $\partial_{zz}\mathbf{v}_z$ can be expressed in terms of seismic velocities and the second-order time derivative of the vertical component of particle velocity $\partial_{tt} v_z$. This results in the following expression for $\partial_z \mathbf{v}_z$ centered at the free surface:

$$\partial_z v_z(\mathbf{x}_0) = \left[\frac{v_z(\mathbf{x}_0+\boldsymbol{\Delta}) - v_z(\mathbf{x}_0)}{\Delta}\right] - \frac{\Delta}{2}\frac{q_p^3 - q_p^3 R_P - p q_s^2 R_S}{q_p - q_p R_P - p R_S}\partial_{tt} v_z(\mathbf{x}_0) + O(\Delta^2). \tag{9}$$

Inserting equation (9) in equation (7) allows equations (6) and (7) to be used as the basis for an inversion scheme aimed at estimating the elastic properties of the near-surface environment. The unknown parameters α and β can be determined by minimizing the following cost function:

$$E_1 = E^{(6)} \times E^{(7)} = \sum_W \left(\frac{\left(L^{(6)} - R^{(6)}\right)}{\left(L^{(6)}\right)^2}\right) \times \sum_W \left(\frac{\left(L^{(7)} - R^{(7)}\right)}{\left(L^{(7)}\right)^2}\right), \tag{10}$$

where $L^{(6)}$, $R^{(6)}$, $L^{(7)}$, and $R^{(7)}$ denote the left and right sides of equations (6) and (7), respectively, and the summations are performed over a space-time window W containing the isolated first arrival. The above strategy requires local estimates of the horizontal slowness p at each of the dense geophone patterns. For noise-free data, this information can be obtained directly from the ratio of the horizontal and temporal derivatives (e.g., $p_x = \partial_x v_i / \partial_t v_i$). In the presence of noise, however, crosscorrelation-based techniques will provide more accurate and stable results.

ESTIMATING OF NEAR-SURFACE SEISMIC MATERIAL PROPERTIES FROM SEA-FLOOR RECORDINGS

Following the approach outlined in the previous section, it is also possible to develop a scheme for extracting the elastic properties of the sea floor from 4-C (three components of particle velocity and pressure) seismic data acquired directly on the seabed. In this case, the boundary conditions allow vertical derivatives of particle velocity to be expressed in terms of horizontal derivatives of particle velocity and pressure. As a result, there exists no need for buried geophones, and the technique is directly applicable to multicomponent seabed data recorded using conventional cable geometries (Figure 1b). Assuming cylindrical symmetry, the recorded data can be transformed to the frequency-wavenumber domain by means of a Fourier-Hankel transformation (Treitel et al., 1982):

$$D(\omega, k) = \int_0^\infty dr\, r\, J_n(kr) \int_{-\infty}^\infty dt \exp(i\omega t)\, d(t, r), \tag{11}$$

where J_n is the Bessel function of the first kind of order n, and $d(t, r)$ and $D(\omega, k)$ denote the data component before and after transformation, respectively. The pressure and the vertical component of particle velocity should be transformed with $n = 0$ and the radial velocity with $n = 1$. Equivalently, the data can also be transformed to the frequency-wavenumber domain with a double Fourier transformation after converting the recorded point-source data to line-source data by means of a spatial filtering operation (Wapenaar et al., 1992). This approach is pursued in the remainder of this paper.

In the following, we assume that the P-wave velocity α_1 and the density ρ_1 of the water layer are constant and known, and that the direct wave is well separated from later arriving reflections and refractions. An incident P-wave Φ_i arriving at the fluid-solid boundary from above will generate a reflected P-wave Φ_r in the water layer and transmitted P- and S-waves Φ_t and Ψ_t, respectively, in the sea floor. The partition of energy between these waves can again be described in terms of reflection and transmission coefficients (de Hoop and van der Hijden, 1985):

$$R_{PP} = \frac{\Phi_r}{\Phi_i} = \frac{(-\rho_1 q_p)/\left(4\rho_2 \beta_2^4 q_w\right) + \Delta_R}{\Delta_{SCH}}, \tag{12}$$

$$T_{PP} = \frac{\Phi_t}{\Phi_i} = \frac{-(\rho_1/\rho_2)\left(p^2 - 1/2\beta_2^2\right)}{\beta_2^2 \Delta_{SCH}}, \tag{13}$$

$$T_{PS} = \frac{\Psi_t}{\Phi_i} = \frac{(\rho_1/\rho_2) p q_p}{\beta_2^2 \Delta_{SCH}}, \tag{14}$$

where R_{PP}, T_{PP}, and T_{PS} are the P-wave reflection coefficient and the P- and S-wave transmission coefficients for potentials, q_p and q_s are defined in equations (3) and (4), and q_w is the vertical slowness of the incident P-wave, defined as $q_w = (\alpha_1^{-2} - p^2)^{1/2}$. The terms Δ_R and Δ_{SCH} are the Rayleigh-wave and Scholte-wave denominators, respectively, given by

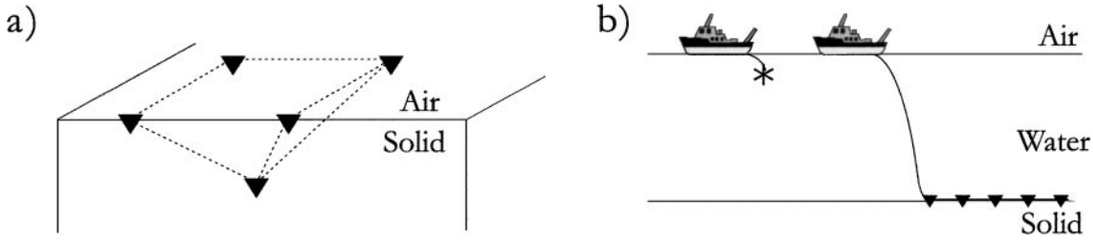

FIG. 1. Acquisition geometries required for the proposed inversion techniques for multicomponent (a) land and (b) seabed data. In (a), the triangles represent 3-C geophones, whereas in (b) they represent combined pressure sensors and 3-C geophones.

de Hoop and van der Hijden (1985):

$$\Delta_R = \left(p^2 - 1/\left(2\beta_2^2\right)\right)^2 + p^2 q_p q_s, \tag{15}$$

$$\Delta_{SCH} = \left(\rho_1 q_p / \left(4\rho_2 q_w \beta_2^4\right)\right) + \Delta_R. \tag{16}$$

Amundsen and Reitan (1995) suggest determining the elastic properties of the sea floor from slowness-dependent estimates of the sea-floor reflection coefficient, which can be obtained from the acoustic pressure P and the vertical component of particle velocity v_z:

$$R_{PP} = \frac{P - (\rho_1/q_w)v_z}{P + (\rho_1/q_w)v_z}. \tag{17}$$

Multicomponent sensor packages deployed on the seabed routinely record three orthogonal components of particle velocity as well as pressure. Consequently, any inversion scheme based exclusively on equation (17) does not benefit fully from the information contained in multicomponent data. By comparison, the following relation between the radial and vertical components of particle velocity can be obtained using a plane-wave approximation (Amundsen and Reitan, 1994):

$$v_h = \frac{-pT_{PP} + q_s T_{PS}}{-q_p T_{PP} - pT_{PS}} v_z, \tag{18}$$

and equation (17) can be rewritten as:

$$P = -\frac{\rho_1(1 + R_{PP})}{q_w(1 - R_{PP})} v_z. \tag{19}$$

The elastic properties of the sea floor can then be estimated by minimizing the following cost function:

$$E_2 = E^{(18)} \times E^{(19)} = \sum_W \left(\frac{(L^{(18)} - R^{(18)})^2}{(L^{(18)})^2} \right) \times \sum_W \left(\frac{(L^{(19)} - R^{(19)})^2}{(L^{(19)})^2} \right), \tag{20}$$

where $L^{(18)}$, $R^{(18)}$, $L^{(19)}$, and $R^{(19)}$ denote the left and right sides of equations (18) and (19). The summation is carried out over the space-time window W containing the isolated direct wave. Since marine seismic sources are highly repetitive, the proposed technique can be applied to common receiver gathers to yield local estimates of the sea-floor properties.

The technique described in this paper is a combination of the methods described in Amundsen and Reitan (1994; 1995). The main advantage of our scheme is that the information contained in all four recorded data components is used simultaneously to estimate the elastic properties of the sea floor. The added value of this combination is illustrated in Figure 2, which shows the magnitude of the relative change of the coefficients in equations (18) and (19) due to a change of +20% in the sea-floor properties from input model parameters of $\alpha_2 = 1700$ m/s, $\beta_2 = 500$ m/s and $\rho_2 = 1200$ kg/m^3. These figures thus provide an indication of the sensitivity of equations (18) and (19) to the sea-floor properties as a function of slowness. Equation (19) is particularly sensitive to the P-wave velocity and to a lesser extent to the density. The S-wave velocity, however, is poorly constrained by this equation and can only be determined when including data propagating at near- or post-critical angles of incidence. In contrast, equation (18) does not only exhibit significant sensitivity to the S-wave velocity at small angles of incidence, but also provides an even better constraint on the P-wave velocity. The density, however, cannot be determined from this equation. Combined inversion of equations (18) and (19), therefore, allows the sea-floor properties to be more accurately determined. Moreover, the S-wave estimate does no longer depend critically on the inclusion of data propagating at high slownesses. The need for acquiring large-offset data in the presence of a deep water layer is therefore reduced.

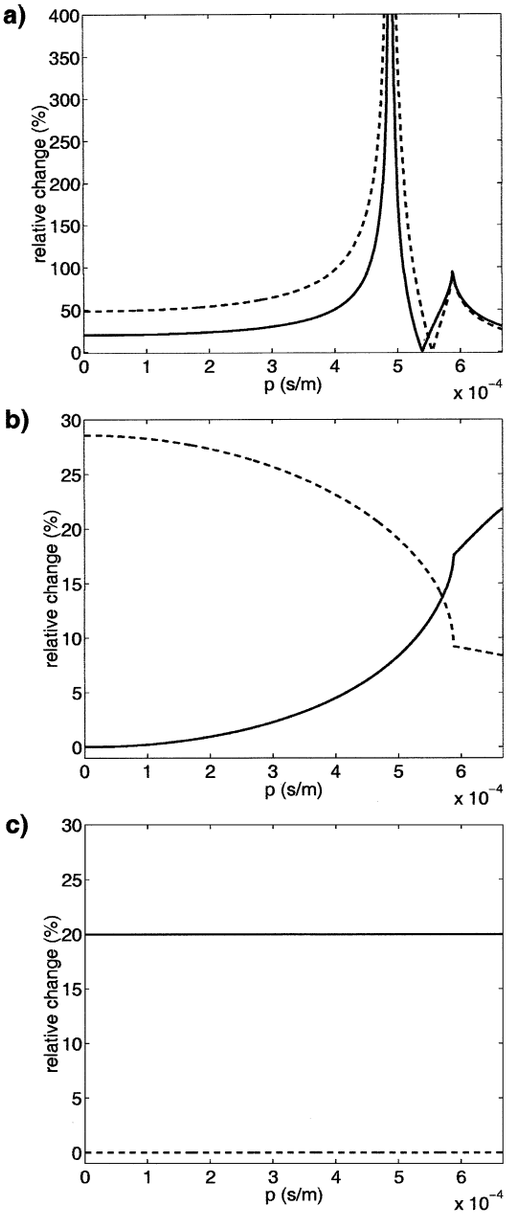

FIG. 2. Relative change of the magnitude of the coefficients in equations (17) (dashed) and (18) (solid) due to a change of +20% in the values of the (a) P-wave velocity α_2, (b) S-wave velocity β_2, and (c) density ρ_2 of the sea floor. The input model parameters are $\alpha_2 = 1700$ m/s, $\beta_2 = 500$ m/s and $\rho_2 = 1200$ kg/m^3.

SYNTHETIC DATA EXAMPLES

We first illustrate the performance of our technique for multicomponent land data. Using a reflectivity code, synthetic data are generated for a horizontally layered model bounded above by a free surface. The P- and S-velocities of the top layer are 1500 m/s and 600 m/s, respectively, and the density is 2000 kg/m^3. Pyramid-shaped receiver configurations (Figure 1a) are deployed along the positive x-axis at intervals of 5 m to a maximum offset of 150 m. Each pyramidal configuration consists of four surface multicomponent (3-C) receivers positioned at the corners of a square with sides of 1-m length. A fifth receiver is buried below the center of the square at a depth of 0.25 m. An explosive point source emitting a 50-Hz Ricker wavelet is located 100 m below the surface, such that the direct-wave energy reaches the receivers at angles of incidence ranging from 0° to 56°. The isolated direct wave that is used for the inversion is shown in Figure 3.

Figure 4 shows cross-sections through cost function E_1 [equation (10)] for source-receiver offsets of 10, 50, and 100 m. The cost function exhibits well-defined minima, such that the near-surface seismic velocities can be estimated using standard minimization techniques. For example, for a source-receiver offset of 50 m, the results are $\alpha = 1490 \pm 130$ m/s and $\beta = 590 \pm 70$ m/s. These estimates are in good agreement with the model parameters. The uncertainty of the results is determined by means of Monte Carlo simulation. For this purpose, band-limited white noise is added to the data, such that the signal-to-noise ratios on the horizontal- and vertical-component data are 20 and 40 dB, respectively. This corresponds to ambient noise levels observed in typical field data. Furthermore, standard errors in the receiver positions and orientations of 5 cm and 2° are assumed. Because the results are particularly sensitive to inaccuracies in the orientation of the buried receiver (Muijs et al., 2002), this

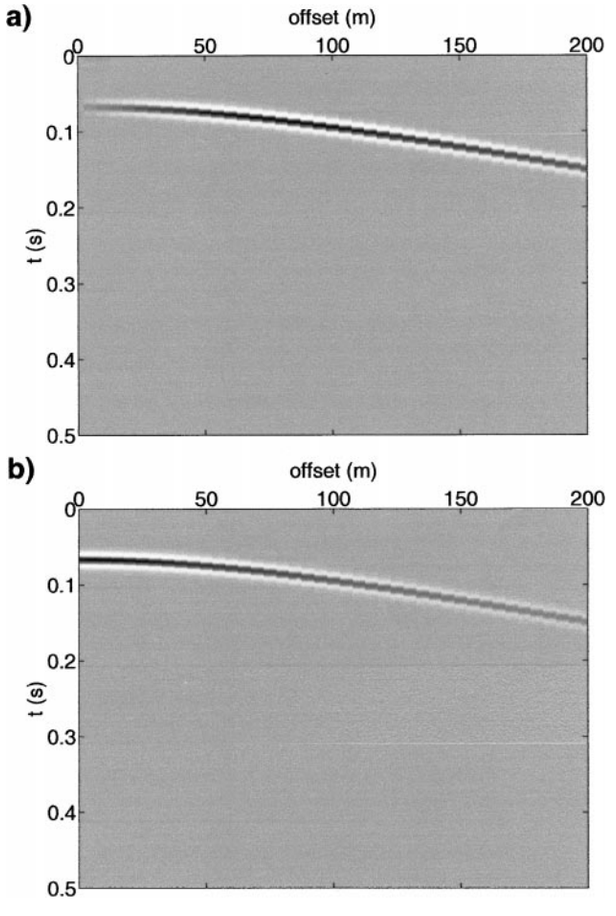

FIG. 3. Synthetic multicomponent land data. Shown are gathers of (a) radial and (b) vertical components of particle velocity recorded by a 3-C surface geophone.

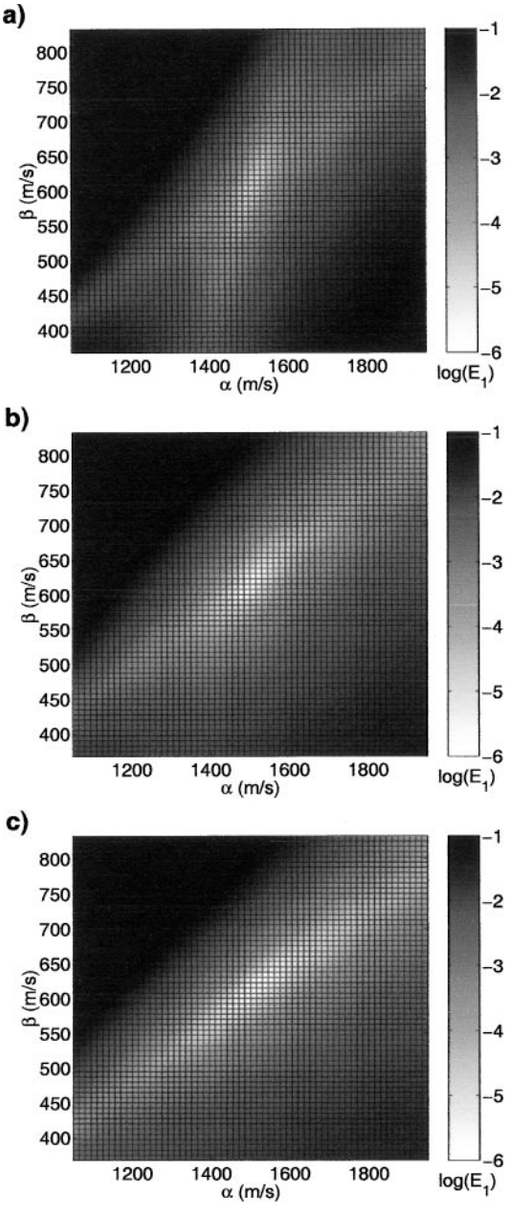

FIG. 4. Cross-sections through cost function E_1 [equation (10)] computed for synthetic land data. Shown are the results calculated for source-receiver offsets of (a) 10 m, (b) 50 m and (c) 100 m. For a source-receiver offset of 50 m, the results are $\alpha = 1490 \pm 130$ m/s and $\beta = 590 \pm 70$ m/s, which compare favorably to the corresponding input model values of 1500 m/s and 600 m/s.

parameter is allowed to vary during the optimization procedure. The above error estimates represent statistical inaccuracies due to deployment-related errors and noise, but unknown systematic errors in the recorded amplitudes have not been considered. Note that the bias of the cost function shown in Figure 4 corresponds to the ratio of the true P- and S-wave velocities.

We also generate synthetic data for an input model consisting of a flat homogeneous sea floor and a 370-m thick water layer. The P- and S-velocities and the density of the sea floor are 1700 m/s, 500 m/s, and 1200 kg/m^3, respectively. An explosive point source emitting a 30-Hz Ricker wavelet is located 5 m below the free surface and is moved along the x-axis with a shot interval of 6.25 m.

Figure 5 shows cross-sections through cost function E_2 as well as its components $E^{(18)}$ and $E^{(19)}$ [equation (20)]. These cross-sections have been computed using data for a source-receiver combination that corresponds to an incidence angle of 20° for the direct wave. Figures 5a and 5b show that the cost functions $E^{(18)}$ and $E^{(19)}$ exhibit distinct preferred directions and, therefore, none of these individual cost functions provides proper constraints for all three desired parameters. Because $E^{(18)}$ and $E^{(19)}$ are biased in different ways, however, the elastic sea-floor properties are much better constrained by the product of these cost functions, which combines the information contained in all recorded data components (Figure 5c).

Cost function E_2 exhibits well-defined minima in each of the three planes, indicating that the sea-floor properties can be accurately estimated. For this source-receiver combination, the results are $\alpha_2^{est} = 1690 \pm 130$ m/s, $\beta_2^{est} = 500 \pm 25$ m/s, and $\rho_2^{est} = 1210 \pm 100$ kg/m^3, with all estimates in good agreement with the input model parameters. The uncertainties are again determined by means of Monte Carlo simulation assuming standard errors of 1 m and 5° in the receiver positions and orientations, respectively. Band-limited white noise is also added to the data, such that the signal-to-noise ratios on the hydrophone and the horizontal- and vertical-component data components correspond to 20, 40, and 50 dB, respectively. These values represent ambient noise levels observed in typical field data. Local estimates of the sea-floor properties could be even better constrained by simultaneously inverting data from several shots in a common receiver gather.

UNSUCCESSFUL APPLICATION TO LAND DATA

The proposed technique for estimating near-surface elastic properties from land data was tested on a multicomponent data set acquired in northern Switzerland. Various types of

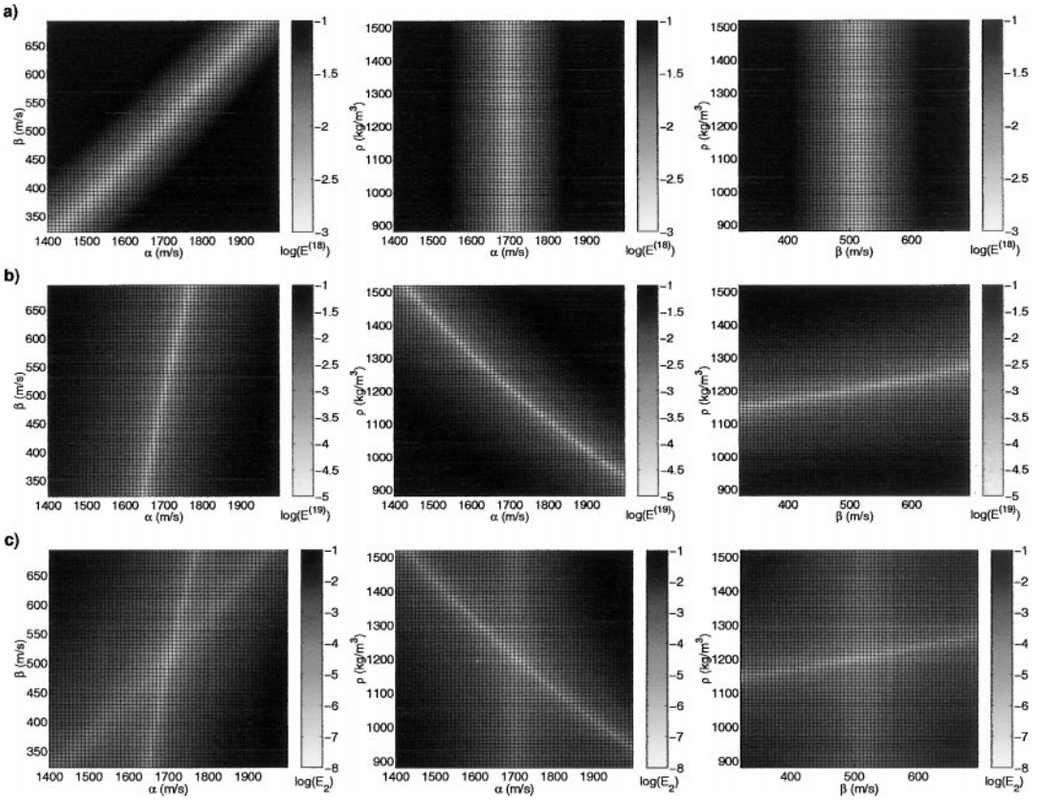

FIG. 5. Cross-sections through the cost functions (a) $E^{(18)}$ (top row), (b) $E^{(19)}$ (middle row), and (c) their product E_2 (bottom row) as defined in equation (20) computed for synthetic seabed data. Shown are the results for P-wave velocity α versus S-wave velocity β (left column), P-wave velocity α versus density ρ (middle column), and S-wave velocity β versus density ρ (right column). These cross-sections are computed for a source-receiver combination that corresponds to an angle of incidence of 20° for the direct wave. The results are $\alpha_2^{est} = 1690 \pm 130$ m/s, $\beta_2^{est} = 500 \pm 25$ m/s, and $\rho_2^{est} = 1210 \pm 100$ kg/m^3, which compare favorably to the corresponding input model values of 1700 m/s, 500 m/s, and 1200 kg/m^3.

receiver configurations, including pyramids and tetrahedrons, were deployed. For all configurations, significant anomalous variations of amplitude and phase were observed between the surface and buried geophones, as well as between the surface geophones themselves. These variations prevented the accurate calculation of spatial wavefield derivatives, such that the elastic properties of the near surface could not be extracted from the acquired data. Figure 6 shows horizontal and vertical components of particle velocity recorded by a pyramidal configuration. The recordings of the buried receiver are shown in red and are in general agreement with synthetic studies. Ideally, the recordings of the four surface geophones should only differ by small phase shifts. The vertical component of particle velocity, therefore, appears to have been recorded reasonably well. In contrast, the horizontal components of particle velocity recorded by the surface geophones exhibit very little coherency, with significant receiver-to-receiver variations in amplitude and phase. Unexpected and unknown changes in coupling and instrument response are the most probable sources of the anomalous variations. Although such variations are only of limited importance in standard seismic surveys, the associated errors are greatly amplified by the finite-difference operators used for calculating the spatial wavefield derivatives in equation (7).

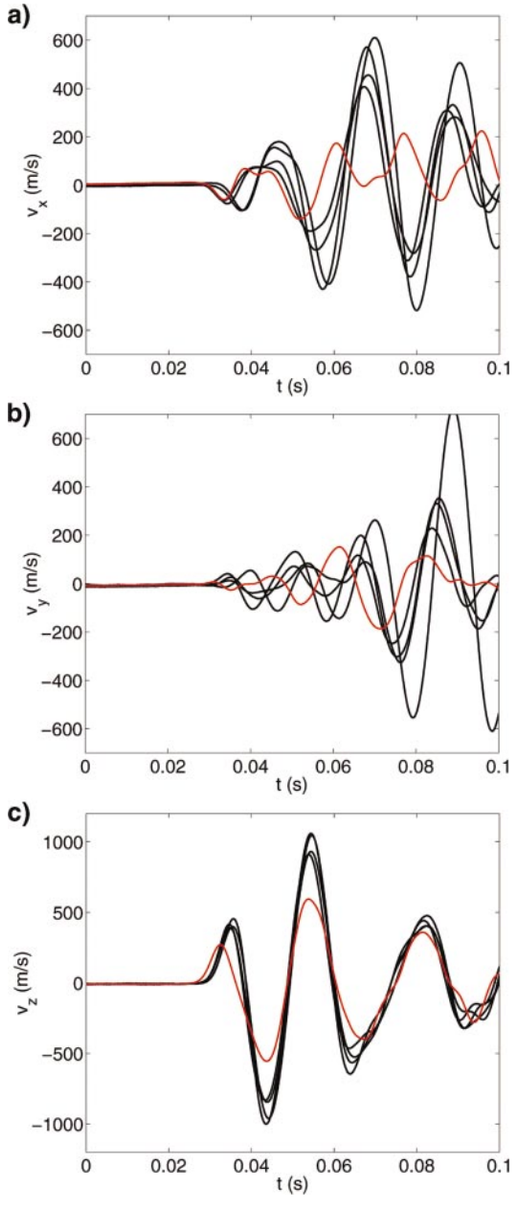

FIG. 6. Multicomponent data recorded by a pyramid-shaped receiver configuration in northern Switzerland. Shown are (a) inline, (b) crossline, and (c) vertical components of particle velocity recorded by the four surface 3-C geophones (black) and the 3-C buried geophone (red). Anomalous variations in the surface horizontal data prevent the accurate computation of spatial wavefield derivatives.

SUCCESSFUL APPLICATION TO SEABED DATA

The proposed method for estimating sea floor properties was tested on a multicomponent (4-C) seabed data set acquired in a northern section of the North Sea. The water depth in this area was approximately 370 m. A shot spacing of 25 m was used. Figure 7 shows receiver gathers for the pressure as well as the vertical and radial components of particle velocity after scaling the raw data with time for display. The source vessel crossed the receiver cable at a distance of 137 m, such that the smallest angle of incidence for the direct wave is approximately 20°. For moderate offsets (<600 m), the direct wave is well separated from later arriving reflected and refracted events. The first arrivals of the 50 shots used for the inversion are outlined by the frame in Figure 7a. Assuming the water layer to be homogeneous, the isolated direct wave was corrected for geometrical spreading by scaling with the square root of time.

The following estimates of the seafloor elastic properties were obtained by minimizing E_2 [equation (20)]: $\alpha_2^{est} = 1630 \pm 10$ m/s, $\beta_2^{est} = 290 \pm 80$ m/s, and $\rho_2^{est} = 1840 \pm 10$ kg/m^3. The uncertainty of the results was determined using Monte Carlo simulation assuming standard errors of 1 m and 5° in the geophone position and orientation, respectively. Band-limited white noise was added to the data, such that the signal-to-noise ratios on the hydrophone and the horizontal- and vertical-component data were 20, 40, and 50 dB, respectively. Again, it should be noted that these uncertainties only reflect statistical errors and that unknown systematic errors cannot be taken into account.

Figure 8 shows cross-sections through cost function E_2 [equation (20)]. In these figures, the third parameter is fixed at the estimated value. The P-wave velocity and density seem to be well constrained, but the S-wave velocity was only poorly constrained, probably because the S-wave velocity is highly sensitive to errors in sensor orientation. Accurate deployment of ocean-bottom acquisition systems is, therefore, essential for obtaining reliable information about this parameter. The refracted wave indicated by the arrows in Figure 7a propagates with an apparent velocity of 1734 m/s, which represents a likely upper limit for the P-wave velocity of the sea floor. The estimated P-wave velocity falls within the range bounded by the sound of speed of water and the velocity of the refracted wave. The inferred density of the sea floor is consistent with laboratory relationships between P-wave velocity and density for a wide variety of unconsolidated seabed sediments (Hamilton,

1980). In contrast, laboratory experiments suggest that the estimated S-wave velocity of 210–370 m/s may be slightly too high, which could be due to systematic errors, such as calibration inaccuracies or poor coupling of the horizontal sensors.

DISCUSSION AND CONCLUSION

We have presented methods for estimating seismic material properties in the immediate vicinity of multicomponent receivers located on land and on the sea floor. Our scheme for shallow land parameters requires data to be recorded in spatially dense configurations of 3-C geophones, of which at least one needs to be buried at a shallow depth below the free surface. By comparison, the proposed scheme for shallow seabed parameters does not require data to be recorded in spatially dense receiver patterns and can be applied to routinely recorded multicomponent ocean-bottom cable data. The methods, which can be applied to individual shot records, provide truly local estimates of the elastic properties of the medium in the immediate vicinity of the geophone groups. In turn, these are the properties required as input for wavefield decomposition schemes (e.g., Wapenaar et al., 1990; Holvik et al.,

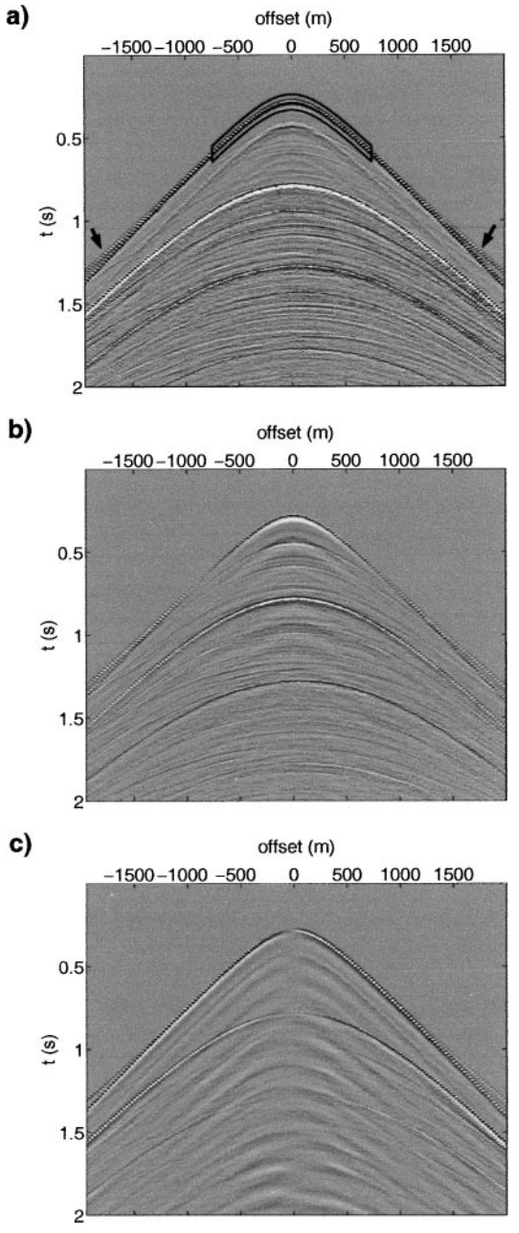

FIG. 7. Receiver gathers of (a) pressure, and (b) vertical and (c) radial component of particle velocity. The signal used for the inversion for sea-floor properties is indicated by the frame in (a). Arrows in (a) indicate a near-surface refracted wave that propagates at an apparent velocity of 1734 m/s.

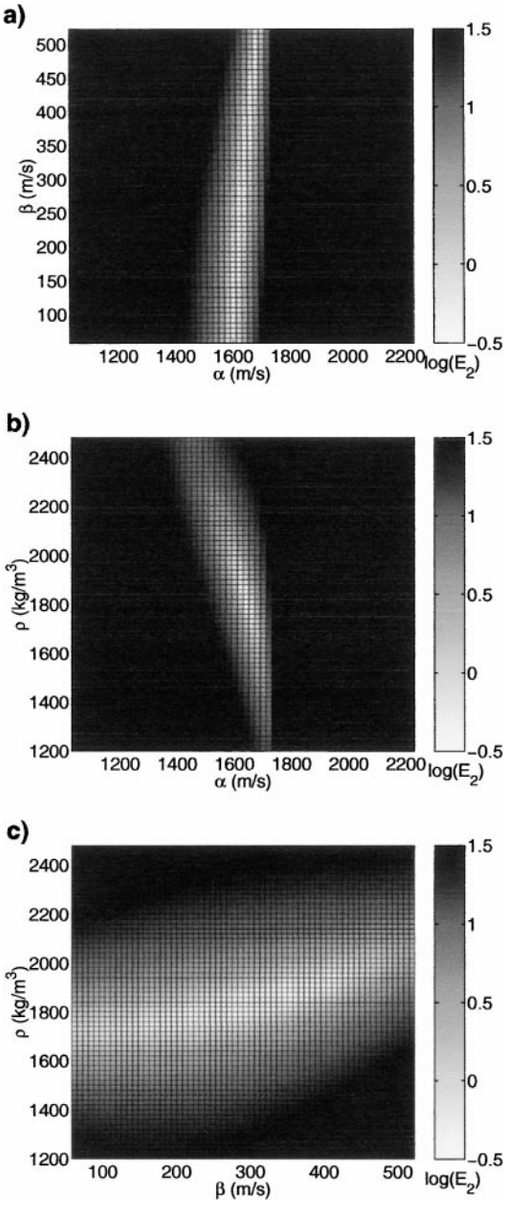

FIG. 8. Cross-sections through the cost function E_2 [equation (19)] computed for observed seabed data. Shown are the results for (a) P-wave velocity α versus S-wave velocity β, (b) P-wave velocity α versus density ρ, and (c) S-wave velocity β versus density ρ. The results are $\alpha_2^{est} = 1630 \pm 10$ m/s, $\beta_2^{est} = 290 \pm 80$ m/s, and $\rho_2^{est} = 1840 \pm 10$ kg/m^3.

1999; Amundsen et al., 2000. Robertsson and Curtis, 2002) and techniques aimed at removing source-side reverberations (e.g., Schalkwijk et al., 2001). Alternatively, such estimates may also be used for static corrections.

The new schemes have been developed under the assumption that the first arrival can be clearly separated from the rest of the data, which is a reasonable approximation if strong scattered energy is not generated just below the air-solid or fluid-solid interface. In regions where the accuracy of the inversion results is significantly affected by near-surface heterogeneities or in the presence of a shallow water layer, the results may be improved by choosing additional data windows that contain isolated phases, such as water-layer multiples or critically refracted waves.

When applied to synthetic data, both methods are robust and yield accurate results as long as sufficient energy is recorded on the horizontal geophones. Unfortunately, the application of the land-based method to multicomponent land data failed, because significant receiver-to-receiver variations in amplitude and phase prevented the accurate computation of wavefield spatial derivatives. Conversely, the proposed sea-floor–based method was successfully applied to a multicomponent data set acquired in the North Sea.

Throughout this paper, we have inherently assumed that the data input to the inversion schemes are good vector representations of the actual ground motion. In reality, receiver-to-receiver variations in coupling or instrument response are likely to introduce systematic errors in the recordings. It is, therefore, anticipated that our estimates, particularly those of the S-wave velocity, would greatly benefit from techniques aimed at improving the vector fidelity of multicomponent data (e.g., Gaiser, 1998; Schalkwijk et al., 1999; Begaini et al., 2000; Strømmen Melbø et al., 2002).

ACKNOWLEDGMENTS

We thank Michael Roth, Robbert van Vossen, and Kabir Roy-Chowdhury for discussions and suggestions, and Alan Green for reviewing the manuscript. This work was supported by Swiss National Science Foundation Grant 2-77593-00. This is ETH contribution 1251.

REFERENCES

Aki, K., and Richards, P. G., 2002, Quantitative seismology, 2nd ed.: University Science Books.

Allnor, R., Čaiti, A., and Arntsen, B., 1997, Inversion of seismic surface waves for shear wave velocities: 68th Ann. Internat. Mtg., Soc. Expl. Geophys., Expanded Abstracts, 1921–1924.

Amundsen, L., Ikelle, L. T., and Martin, J., 2000, Multiple attenuation and P/S splitting of multicomponent obc data at a heterogeneous sea floor: Wave Motion, **32**, 67–78.

Amundsen, L., and Reitan, A., 1994, AVO estimation of water-bottom P- and S-wave velocities from the particle velocity field: J. Seis. Expl., **3**, 231–243.

——— 1995, Estimation of sea-floor wave velocities and density from pressure and particle velocity by AVO analysis: Geophysics, **60**, 1575–1578.

Bagaini, C., Bale, R., Caprioli, P., Muyzert, E., and Ronen, S., 2000, Assessment and calibration of horizontal geophone fidelity in seabed-4C using shear waves: 62nd Mtg., Eur. Assn. Geosci. Eng., session L0002.

Caldwell, J., 1999, Marine multicomponent seismology: The Leading Edge, **18**, 1274–1282.

Curtis, A., and Robertsson, J., 2002, Volumetric wavefield recording and near-receiver group velocity estimation for land seismics: Geophysics, **67**, 1602–1611.

de Hoop, A. T., and van der Hijden, J. H. M., 1985, Seismic waves generated by an impulsive point source in a solid/fluid configuration with a plane boundary: Geophysics, **50**, 1083–1090.

Gaiser, J. E., 1998, Compensating OBC data for variations in geophone coupling: 68th Ann. Internat. Mtg., Soc. Expl. Geophys., Expanded Abstracts, 1429–1432.

Hamilton, E. L., 1980, Geoacoustic modeling of the sea floor: J. Acous. Soc. Am., **68**, 1313–1340.

Haugen, G. U., Pedersen, A. S., and Osen, A., 1998, Processing and interpretation of the Gullfaks SUMIC ocean bottom data: 64th Mtg., Eur. Assn. Geosci. Eng., session 03–37.

Holvik, E., Osen, A., Amundsen, L., and Reitan, A., 1999, On P- and S-wave separation at a liquid-solid interface: J. Seis. Expl., **8**, 91–100.

Muijs, R., Holliger, K., and Robertsson, J. O. A., 2000, Effects of deployment-related inaccuracies on explicit P/S-wave separation: 62nd Mtg., Eur. Assn. Geosci. Eng., session L0049.

——— 2002, Perturbation analysis for an explicit wavefield separation scheme for P- and S-waves: Geophysics, **67**, 1972–1982.

Muyzert, E., 2000, Scholte wave velocity inversion for a near surface S-velocity model and P-S-statics: 70th Ann. Internat. Mtg., Soc. Expl. Geophys., Expanded Abstracts, 1197–1200.

Robertsson, J. O. A., and Curtis, A., 2002, Wavefield separation using densely deployed three-component single-sensor groups in land surface-seismic recordings: Geophysics, **67**, 1624–1633.

Robertsson, J. O. A., and Muyzert, E., 1999, Wavefield separation using a volume distribution of three component recordings: Geophys. Res. Lett., **26**, 2821–2824.

Roth, M., and Holliger, K., 1999, Inversion of source-generated noise in high-resolution seismic data: The Leading Edge, **18**, 1402–1406.

Schalkwijk, K. M., Wapenaar, C. P. A., and Verschuur, D. J., 1999, Application of two-step decomposition to multicomponent ocean-bottom data: Theory and case study: J. Seis. Expl., **8**, 261–278.

Schalkwijk, K., Verschuur, D. J., and Wapenaar, C. P. A., 2001, A decomposition and multiple removal strategy for multicomponent OBC data: 71st Ann. Internat. Mtg., Soc. Expl. Geophys., Expanded Abstracts, 813–816.

Strømmen Melbø, A., Robertsson, J., and Van Manen, D. J., 2002, PZ calibration using critically refracted waves: 64th Mtg., Eur. Assn. Geosci. Eng., session A008.

Treitel, S., Gutowski, P. R., and Wagner, D. E., 1982, Plane-wave decomposition of seismograms: Geophysics, **47**, 1375–1401.

Wapenaar, C. P. A., Herrmann, P., Verschuur, D. J., and Berkhout, A. J., 1990, Decomposition of multicomponent seismic data into primary P- and S- wave responses: Geophys. Prosp., **38**, 633–662.

Wapenaar, C. P. A., Verschuur, D. J., and Herrmann, P., 1992, Amplitude preprocessing of single- and multicomponent seismic data: Geophysics, 57, 1178–1188.